Radiolytic formation of the carbon dioxide radical anion in acetonitrile revealed by transient IR spectroscopy

Journal:	*Physical Chemistry Chemical Physics*
Manuscript ID	CP-ART-02-2018-000977.R1
Article Type:	Paper
Date Submitted by the Author:	24-Mar-2018
Complete List of Authors:	Grills, David; Brookhaven National Laboratory, Chemistry Lymar, Sergei; Brookhaven National Laboratory, Chemistry

Journal Name

ARTICLE

Radiolytic formation of the carbon dioxide radical anion in acetonitrile revealed by transient IR spectroscopy

Received 00th January 20xx,
Accepted 00th January 20xx

DOI: 10.1039/x0xx00000x

www.rsc.org/

David C. Grills* and Sergei V. Lymar*

The solvated electron in CH_3CN is scavenged by CO_2 with a rate constant of 3.2×10^{10} M^{-1} s^{-1} to produce the carbon dioxide radical anion ($CO_2^{\bullet-}$), a strong and versatile reductant. Using pulse radiolysis with time-resolved IR detection, this radical is unambiguously identified by its absorption band at 1650 cm^{-1} corresponding to the antisymmetric $CO_2^{\bullet-}$ stretch. This assignment is confirmed by ^{13}C isotopic labelling experiments and DFT calculations. In neat CH_3CN, $CO_2^{\bullet-}$ decays on a ~10 μs time scale via recombination with solvent-derived radicals ($R^\bullet$) and solvated protons. Upon addition of formate (HCO_2^-), the radiation yield of $CO_2^{\bullet-}$ is substantially increased due to H-atom abstraction by $R^\bullet$ from HCO_2^- ($R^\bullet + HCO_2^- \rightarrow RH + CO_2^{\bullet-}$), which occurs in two kinetically separated steps. The rapid step involves the stronger H-abstracting $CN^\bullet$, $CH_3^\bullet$, and possibly, $H^\bullet$ primary radicals, while the slower step is due to the less reactive, but more abundant radical, $CH_2CN^\bullet$. The removal of solvent radicals by HCO_2^- also results in over a hundredfold increase in the $CO_2^{\bullet-}$ lifetime. $CO_2^{\bullet-}$ scavenging experiments suggest that at 50 mM HCO_2^-, about 60% of the solvent-derived radicals are engaged in $CO_2^{\bullet-}$ generation. Even under CO_2 saturation, no formation of the radical adduct, $(CO_2)_2^{\bullet-}$, could be detected on the microsecond time scale.

1. Introduction

In the gas phase, the carbon dioxide radical anion ($CO_2^{\bullet-}$) is unstable toward electron autodetachment, and the equilibrium,

$$CO_2 + e^- \rightleftharpoons CO_2^{\bullet-} \qquad \Delta G^0$$

lies to the left, with $\Delta G^0 \approx 15$ kcal/mol[1] based on the CO_2 electron affinity, $EA \approx -0.6$ eV.[2] However, condensed media tend to stabilize $CO_2^{\bullet-}$ much more strongly than the excess electron. Even in solvents with dielectric constants of less than 2, the above equilibrium is shifted to the right, with ΔG^0 ranging from –7 to –13 kcal/mol, as has been deduced from pulse radiolysis/transient conductivity studies.[3-5] In the highly polar aqueous environment, ΔG^0 further decreases to –23 kcal/mol,[6] and water remains the only solvent in which $CO_2^{\bullet-}$ has been unambiguously identified by UV-Vis,[7-10] ESR,[11] and resonance Raman[12] transient spectroscopies.

Although a weaker reductant than the hydrated electron, $CO_2^{\bullet-}$ is still strongly reducing ($E°(CO_2/CO_2^{\bullet-}) = -2.14$ and -2.21 V in water[13] and dimethylformamide,[14] respectively, vs SCE) and substantially more selective and long-lived. These properties have engendered an extensive application of $CO_2^{\bullet-}$ as a versatile reductant in kinetic and mechanistic studies using pulse radiolysis in water,[15,16] where $CO_2^{\bullet-}$ can be generated through both reduction of dissolved CO_2 with the solvated electrons (e_s^-),

$$CO_2 + e_s^- \xrightarrow{k_{CO2}} CO_2^{\bullet-} \qquad (1)$$

and oxidation of the formate ion (HCO_2^-).[17] The latter method is based on formate's ability to scavenge the radiolytically-generated radicals, $OH^\bullet$ and $H^\bullet$,

$$OH^\bullet/H^\bullet + HCO_2^- \longrightarrow H_2O/H_2 + CO_2^{\bullet-} \qquad (2)$$

and has the added benefit of providing a cleaner system for mechanistic studies by eliminating these rather indiscriminately reactive radicals.

In this work, we explore the radiolytic production of $CO_2^{\bullet-}$ in the polar aprotic solvent, acetonitrile (CH_3CN), which includes both direct CO_2 reduction by e_s^- and use of solvent-derived radicals for H-atom abstraction from HCO_2^- by analogy with reaction (2). Specifically, we aim at direct, definitive, spectroscopic detection of $CO_2^{\bullet-}$, maximizing its yield, and characterizing its formation and decay kinetics. As a principal tool for these studies, we employ the recently-developed technique of pulse radiolysis combined with time-resolved IR spectroscopy (PR-TRIR) in liquid samples.[18,19]

Our interest in this subject matter arises primarily from the utility of CH_3CN and pulse radiolysis for investigating redox reactions in an aprotic environment. Due to its excellent solubilizing propensity and large electrochemical window, CH_3CN is one of the most widely used solvents in redox catalysis, and pulse radiolysis is a versatile method for generating catalytic intermediates.[20,21] These factors, and its good mid-IR transparency, have made CH_3CN a solvent of choice for PR-TRIR work on the dynamics of redox catalysis in our group.[22,23,21,19]

The properties and reactivity of $CO_2^{\bullet-}$ in CH_3CN are also of importance for understanding electrochemical CO_2 reduction

---

Chemistry Division, Brookhaven National Laboratory, P.O. Box 5000, Upton, NY 11973-5000, USA. E-mail: dcgrills@bnl.gov, lymar@bnl.gov

† Electronic Supplementary Information (ESI) available: (1) Additional experimental detail, (2) supplemental data, including rate constant measurements, and (3) thermodynamic calculations. See DOI: 10.1039/x0xx00000x

in this and other aprotic solvents.[24-29] Although $CO_2^{\bullet-}$ has been invoked as a key intermediate, it has not, with one possible exception,[24] been detected. In that work, the UV absorption bands appearing in CH_3CN and propylene carbonate upon applying cathodic currents, revealed by modulated specular reflectance spectroscopy, were assigned to free $CO_2^{\bullet-}$ in the catholyte. In the present study, we have used PR-TRIR to obtain a definitive spectroscopic identification of $CO_2^{\bullet-}$ in CH_3CN, via its antisymmetric stretching vibration.

Although the current understanding of CH_3CN radiation chemistry leaves much to be desired, the basic features that have emerged from previous studies[30-40] are summarized in Scheme 1. As with other solvents, the early radiolysis events consist of solvent ionization and electronic excitation that are clustered into radiation spurs containing e_s^-, solvent holes ($CH_3CN^{\bullet+}$), and excited solvent molecules ($^*CH_3CN$). The subsequent rapid processes include diffusional spur expansion, geminate electron-hole recombination producing additional $^*CH_3CN$, deactivation of $^*CH_3CN$ and its fragmentation along the weakest C–H and C–C bonds (bond dissociation energies of ~97 and ~125 kcal/mol, respectively[41]), and an ion-molecular reaction of $CH_3CN^{\bullet+}$ with solvent. The latter may occur either through acid dissociation of $CH_3CN^{\bullet+}$ or by H-atom abstraction from CH_3CN, which are indistinguishable in that they yield the same products; namely, $CH_2CN^{\bullet}$ and the solvated proton (CH_3CNH^+), as shown by reaction (3) in Scheme 1b). The $CH_3^{\bullet}$ and $CN^{\bullet}$ primary radicals are thermodynamically capable of abstracting an H atom from CH_3CN (reactions (4) and (5); Table 1), which would further contribute to the $CH_2CN^{\bullet}$ yield, making $CH_2CN^{\bullet}$ the predominant solvent radical in solution. Although $H^{\bullet}$ can also abstract an H atom from solvent (reaction (6a); Table 1), this reaction is much slower than $H^{\bullet}$ addition across the solvent's C≡N bond (reaction (6b)).[30,42,43] A computational study has suggested that C-addition is less activated than N-addition, and that $CH_3C(H)N^{\bullet}$ is more stable than $CH_3CNH^{\bullet}$.[44]

It has been shown that in liquid CH_3CN, the conventional cavity-solvated electrons absorbing at 1450 nm co-exist in equilibrium with dimer radical anions comprised of two solvent molecules, $(CH_3CN)_2^{\bullet-}$, that absorb in the 500-600 nm region.[37,45-48] The equilibrium is established on a ~100 ps time scale and was originally estimated to favor the dimer by a factor of 1.3 at room temperature,[45] but this factor has since been reevaluated as ~4.[47,48] Although the reactivity of these two reducing species toward electron-accepting solutes may differ, in many cases, including those considered here, this difference is inconsequential due to the rapidity of equilibration, and herein we will refer to both reducing species in CH_3CN collectively as a solvated electron (e_s^-).

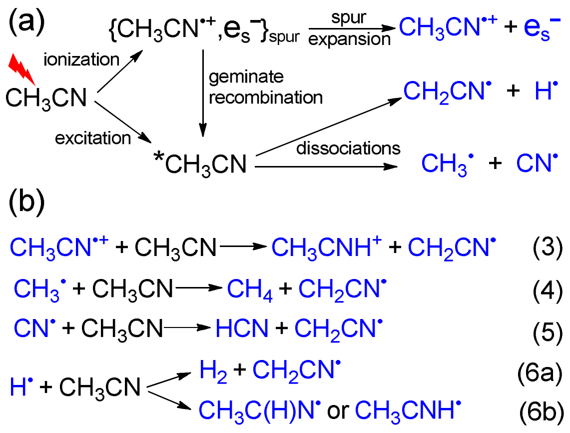

Scheme 1 (a) Early radiolysis events in CH_3CN leading to the solvated electron and primary solvent-derived radicals ($R^{\bullet}$). (b) Reactions of primary radicals with solvent; the CH_3CNH^+ product of reaction (3) is equivalent to the solvated proton.

Table 1 Gas-phase bond dissociation energies (BDE, kcal/mol) in $H\text{-}CO_2^-$ and the products (H-R) of H-atom abstraction by solvent-derived radicals ($R^{\bullet}$) shown in Scheme 1a.

Species	$H\text{-}CO_2^-$	$H\text{-}CH_2CN$	H-H	$H\text{-}CH_3$	H-CN	$CH_3CN\text{-}H^+$
BDE[a]	86[b]	97[c]	104.15	105.0[d]	126.3[e]	154
ΔBDE[f]	0	11	18	19	40	68

[a] Averaged or selected values from a literature compilation,[41] except those for $H\text{-}CO_2^-$ and $CH_3CN\text{-}H^+$ that are derived in the ESI sections 4 and 5, respectively; [b] ±5; [c] ±1; [d] ±0.1; [e] ±0.2; [f] Relative to $H\text{-}CO_2^-$, $\Delta BDE \approx -\Delta_{R7}H^0$.

Radiation yields of e_s^- that survive geminate and spur recombination (Scheme 1a) ranging from $G(e_s^-) = 1$ to 2 electrons/100 eV have been deduced from e_s^- scavenging experiments[33,34,37,49,50] with an average value of $G(e_s^-) = 1.5 \pm 0.5$ (Table S1). The individual radiation yields of the primary solvent-derived radicals (Scheme 1a) are more uncertain. However, their combined yield of $G(R^{\bullet}) \approx 7$ radicals/100 eV gleaned from total radical scavenging studies[51,30] is much larger than $G(e_s^-)$. This assertion is supported by end-product analyses upon radiolysis of liquid CH_3CN.[52,30,31]

2. Experimental methods

Materials and sample preparation. CH_3CN and CD_3CN were purified and dried by refluxing over KBH_4, followed by degassing and vacuum transfer onto activated 3Å molecular sieves. Tetrabutylammonium formate ($[^nBu_4N][HCO_2]$) and its ^{13}C-labeled analogue ($[^nBu_4N][H^{13}CO_2]$) were synthesized by a previously published procedure[23] or a slightly modified version of it, and *fac*-ReCl(bpy)$(CO)_3$ was synthesized as previously described.[53] Samples were prepared in a nitrogen-filled glovebox. CO_2 or $^{13}CO_2$, diluted by inert gas, was introduced into solutions by bubbling at ambient pressure. The concentration of dissolved CO_2 was assigned using the published solubility in dry CH_3CN (280 mM/atm).[54] TRIR experiments involving $^{13}CO_2$ and $H^{13}CO_2^-$ required the use of CD_3CN solvent (see ESI section 1 for detail).

Pulse radiolysis. The pulse radiolysis experiments were performed at either (i) the BNL Laser Electron Accelerator Facility (LEAF) using 8.7 MeV electron pulses of <50 ps duration (for vis/near-IR detection) and ~7 ns duration (for TRIR detection), or (ii) a Van de Graaff accelerator using 2 MeV electron pulses of 200-500 ns duration (for UV/vis detection) and 2 μs duration (for step-scan FTIR detection). Dosimetry for the UV/vis Van de Graaff experiments was performed with an N_2O-saturated 10 mM KSCN aqueous solution using $G\varepsilon = 4.87\times10^4$ ions $(100\ eV)^{-1}\ M^{-1}\ cm^{-1}$ for $(SCN)_2^{\bullet-}$ at 472 nm. A solvent density correction was made when applying this dosimetry to pulse radiolysis in CH_3CN.

Additional details of sample preparation, computational methods, and pulse radiolysis experiments are provided in the ESI section 1.

3. Results and discussion

3.1 Generating $CO_2^{\bullet-}$ through e_s^- capture

Monitoring at 1460 nm, near the λ_{max} of e_s^- (Fig. S1), we have observed a gradual e_s^- lifetime decrease upon increasing CO_2 concentration (Fig. S2). This result is attributable to the capture of e_s^- by CO_2 to generate $CO_2^{\bullet-}$ (reaction (1)), with a second-order rate constant $k_{CO2} = 3.2 \times 10^{10}\ M^{-1}\ s^{-1}$, which is close to the diffusion-controlled limit in CH_3CN. However, our attempts to detect $CO_2^{\bullet-}$ through its characteristic UV absorption ($\lambda_{max} \approx$ 220-240 nm in water[7,9,55]) have met with considerable difficulty. As shown by Fig. S3, a broad featureless transient absorption due to a medley of solvent-derived radicals strongly obscures absorption by any other species below 350 nm. However, we do observe the appearance of some additional absorption around 275 nm upon saturating CH_3CN with 10% CO_2 that could belong to $CO_2^{\bullet-}$, provided its spectrum is ~40 nm red-shifted from that in water (Fig. S3). The only support for this tentative assignment comes from the spectroelectrochemical observations of Aylmer-Kelly et al.[24]

For an unambiguous $CO_2^{\bullet-}$ detection we have turned to the structurally-sensitive technique of TRIR spectroscopy.[18] In cryogenic noble gas matrices, the antisymmetric stretch of $CO_2^{\bullet-}$ has previously been observed as an IR band at 1657-1658 cm^{-1},[56-58] while in room temperature solid alkali halide it appeared at 1665 cm^{-1} after gamma irradiation of trapped formate.[59,60] Indeed, Fig. 1a shows that the TRIR spectrum recorded promptly after pulse radiolysis of CH_3CN containing 28 mM CO_2 exhibits an absorption band at 1650 cm^{-1}. This band, which we assign to $CO_2^{\bullet-}$, is formed within the ~40 ns rise time of our TRIR detection system[18] and is not observed in the absence of CO_2. This assignment has been verified using ^{13}C-labeled CO_2. As shown in Fig. 1a this isotopic substitution results in the transient IR band shifting to 1605 cm^{-1}. This 45 cm^{-1} shift is identical to the isotopic shift predicted for the antisymmetric stretch of $CO_2^{\bullet-}$ by Density Functional Theory (DFT) calculations (ESI section 2) and is also close to the isotopic shift of 44 cm^{-1} observed in matrix isolation studies.[56,58] These results confirm the assignment of the 1650 and 1605 cm^{-1} transient bands to the antisymmetric stretches of $^{12}CO_2^{\bullet-}$ and $^{13}CO_2^{\bullet-}$, respectively, and provide direct, unambiguous evidence for the formation of $CO_2^{\bullet-}$ in CH_3CN via the capture of e_s^- by CO_2.‡

3.2 Generating $CO_2^{\bullet-}$ via scavenging solvent-derived radicals

We[23] and others[35] have previously obtained evidence for the radiation-induced generation of a reducing species in addition to e_s^- in CH_3CN solutions containing formate ions (HCO_2^-) and conjectured that this species is, in fact, $CO_2^{\bullet-}$ produced by H-atom abstraction reactions between the solvent-derived radicals (collectively denoted $R^\bullet$) and HCO_2^-,

$$R^\bullet + HCO_2^- \longrightarrow RH + CO_2^{\bullet-} \qquad (7)$$

Based on the BDEs in Table 1, reaction (7) is thermodynamically favorable, albeit to varying degree, for all primary $R^\bullet$. To substantiate the occurrence of reaction (7), we have recorded TRIR spectra following pulse radiolysis of a 50 mM solution of $H^{13}CO_2^-$. As shown in Fig. 1a, the band at 1605 cm^{-1} due to $^{13}CO_2^{\bullet-}$ is formed promptly after the electron pulse. The prompt TRIR spectrum obtained with 50 mM $H^{13}CO_2^-$ and 28 mM $^{12}CO_2$ exhibits bands of both $^{12}CO_2^{\bullet-}$ and $^{13}CO_2^{\bullet-}$, which allows spectroscopic separation of the two $CO_2^{\bullet-}$ formation pathways (reactions (1) and (7)) and evaluation of their relative contributions (Fig. 1b).

The appearance of the 1650 and 1605 cm^{-1} absorption bands upon pulse radiolysis of solutions containing $^{12}CO_2/H^{12}CO_2^-$ and $^{13}CO_2/H^{13}CO_2^-$, respectively, has also been detected using a time-resolved step-scan FTIR spectroscopic technique (Fig. S4).

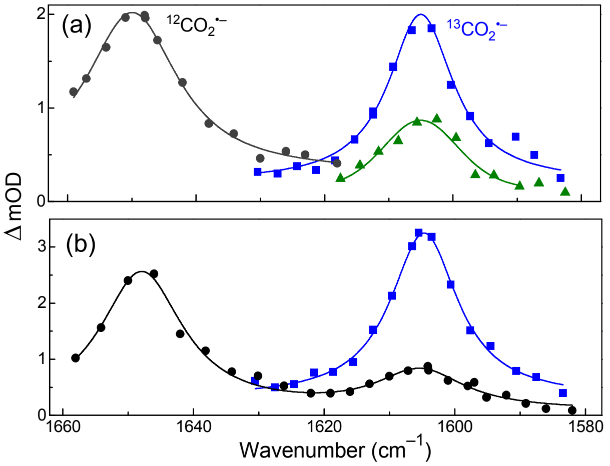

Fig. 1 TRIR spectra recorded 60 ns after 7 ns pulse radiolysis of deoxygenated acetonitrile solutions and normalized for radiation dose. Panel (a): 28 mM $^{12}CO_2$ in CH_3CN (●, ν_{max} = 1650 cm^{-1}, A_{max} = 2.0 mOD); 28 mM $^{13}CO_2$ in CD_3CN (■, ν_{max} = 1605 cm^{-1}, A_{max} = 2.0 mOD); 50 mM $H^{13}CO_2^-$ in CD_3CN (▲, ν_{max} = 1605 cm^{-1}, A_{max} = 0.8 mOD). Panel (b): 28 mM $^{12}CO_2$ and 50 mM $H^{13}CO_2^-$ in CD_3CN (●, ν_{max} = 1650 cm^{-1}, A_{max} = 2.6 mOD and ν_{max} = 1605 cm^{-1}, A_{max} = 0.8 mOD); 28 mM $^{13}CO_2$ and 50 mM $H^{13}CO_2^-$ in CD_3CN (■, ν_{max} = 1605 cm^{-1}, A_{max} = 3.3 mOD).

3.3 Kinetics and yields

Kinetics and yields are related, as evidenced by Fig. 2. When CO_2 is the only solute, the IR absorption of promptly formed $CO_2^{\bullet-}$ rapidly decays with kinetics that is close to second-order ($t_{½}$ = 1.9 and $t_{¼}$ = 5.3 μs). This decay is, we believe, primarily due to the reactions of $CO_2^{\bullet-}$ with the more abundant solvent-derived $CH_2CN^\bullet$ and $CH_3C(H)N^\bullet$. The former may occur either by simple addition, producing stable 2-cyanoacetate ($NCCH_2CO_2^-$), or by electron transfer, yielding CO_2 + CH_2CN^-. Indeed, our estimates for $E^0(CH_2CN^{\bullet/-})$ range from −0.04 to 0.22 V vs SCE (ESI section 5), which suggests that $CH_2CN^\bullet$

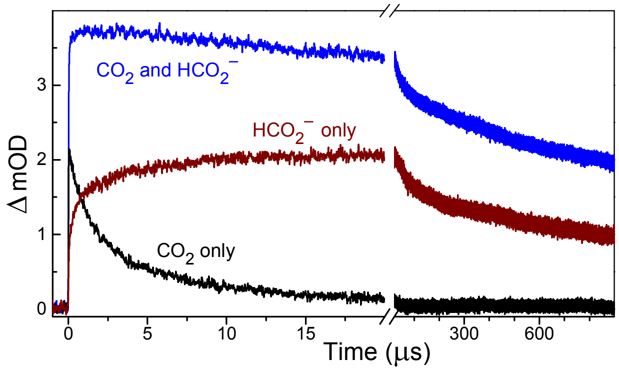

Fig. 2 TRIR kinetic traces of $^{13}CO_2^{\bullet-}$ absorption normalized for radiation dose and recorded at 1605 cm^{-1} after 7 ns pulse radiolysis of deoxygenated CD_3CN containing: 28 mM $^{13}CO_2$ (black); 50 mM $H^{13}CO_2^-$ (wine); 28 mM $^{13}CO_2$ and 50 mM $H^{13}CO_2^-$ (blue). For all traces, the initial rise rate is limited by the ~40 ns IR detection time resolution. The absorption decay half-lives are 1.9 µs (CO_2 only), 800 µs (HCO_2^- only), and >1 ms (CO_2 and HCO_2^-). Note the time axis scale change at 20 µs.

should be readily reducible by $CO_2^{\bullet-}$. For the $CO_2^{\bullet-}$ + $CH_3C(H)N^{\bullet}$ reaction, H-atom transfer appears to be the likely pathway. It has been calculated that the H atom is extremely weakly bound to the CN group (BDE ≈ 19 kcal/mol),[44] which makes the $CO_2^{\bullet-}$ + $CH_3C(H)N^{\bullet}$ = HCO_2^- + CH_3CN reaction exothermic by ~67 kcal/mol. Other reactions contributing to $CO_2^{\bullet-}$ absorption decay are the concurrent $CO_2^{\bullet-}$ + $CO_2^{\bullet-}$ radical-radical and $CO_2^{\bullet-}$ + CH_3CNH^+ acid-base recombinations; the latter would preserve the radical, yielding $HCO_2^{\bullet}$, but destroy the $CO_2^{\bullet-}$ IR band. For more on the $CO_2^{\bullet-}$ decay pathways see ESI section 6.

When CO_2 is replaced by HCO_2^-, an entirely different biphasic kinetic pattern of $CO_2^{\bullet-}$ formation emerges. It consists of a prompt rise followed by a slower accumulation, but no decay occurs on a 20 µs time scale (Fig. 2). This pattern is explicable in terms of reaction (7) where the prompt rise is due to the more strongly H-abstracting solvent-derived radicals, namely, $CN^{\bullet}$, $CH_3^{\bullet}$, and possibly, $H^{\bullet}$, for which reaction (7) has standard enthalpies of $\Delta_{R7}H^0$ ≈ −40, −19, and −18 kcal/mol, respectively (Table 1). The efficacy of $CO_2^{\bullet-}$ generation by these reactions depends on their competition with reactions (4)-(6), and at 50 mM HCO_2^-, the prompt $CO_2^{\bullet-}$ yield amounts to ~40% of that observed in the CO_2-only solution (Fig. 2).

Despite the very large exothermicity of reaction (7) for $CH_3CN^{\bullet+}$, $\Delta_{R7}H^0$ ≈ −68 kcal/mol, its significant participation in the prompt formation of $CO_2^{\bullet-}$ appears doubtful. As detailed in the ESI section 5, we estimate the consumption of $CH_3CN^{\bullet+}$ by the solvent through reaction (3) to be nearly 60 kcal/mol exothermic due to the extreme acidity (pK_a ≈ −45) and H-atom affinity (~154 kcal/mol) of this radical, which should make this reaction exceedingly rapid, possibly occurring on the time scale of the thermal equilibration of $CH_3CN^{\bullet+}$. Indeed, reaction (3) is analogous to the immeasurably rapid $H_2O^{\bullet+}$ + H_2O → H_3O^+ + $OH^{\bullet}$ process in water. It thus appears unlikely that the strongly H-atom accepting and one-electron oxidizing $CH_3CN^{\bullet+}$ ($E^0(CH_3CN^{\bullet+/0})$ ≈ 4.6 V in CH_3CN vs SCE, ESI section 5) is sufficiently long-lived to engage in redox reactions with solutes at ordinary concentrations, as has been suggested in several papers.[61-64]

In contrast to the CO_2-only conditions, a growth of $CO_2^{\bullet-}$ absorption in the HCO_2^--only solution is observed over the next 20 µs, which more than doubles the apparent $CO_2^{\bullet-}$ yield (Fig. 2). We attribute this additional $CO_2^{\bullet-}$ production to reaction (7) with $R^{\bullet}$ being the weaker H-atom abstracting but much more abundant radical, $CH_2CN^{\bullet}$ ($\Delta_{R7}H^0$ ≈ −11 kcal/mol, Table 1). Apparently, this reaction outcompetes all $CO_2^{\bullet-}$ decay modes until $CH_2CN^{\bullet}$ is depleted (at ~20 µs), and the $CO_2^{\bullet-}$ recombination reactions take over, causing its slow decay on the sub-millisecond time scale.

With both 28 mM CO_2 and 50 mM HCO_2^- present, the IR absorption amplitude of the promptly produced $CO_2^{\bullet-}$ is ~18% greater than the sum of the prompt amplitudes in the CO_2-only and HCO_2^--only solutions (Figs. 1 and 2). At lesser HCO_2^- concentrations, this effect is reduced and more difficult to ascertain. The data for the $^{12}CO_2/H^{13}CO_2^-$ solution in Fig. 1b show that this enhancement comes entirely from the ~30% increase in the $^{12}CO_2^{\bullet-}$ yield compared to the $^{12}CO_2$-only solution, while the $^{13}CO_2^{\bullet-}$ is unchanged compared to the $H^{13}CO_2^-$-only solution, which can only occur if the yields of scavengeable e_s^- and attendant contribution of reaction (1) are increased by this amount in the presence of formate. This interpretation is supported by a comparison of the e_s^- absorption amplitudes at 1460 nm following pulse radiolysis of deoxygenated CH_3CN with and without added HCO_2^- (Fig. S5) that reveals a ~35% increase of e_s^- yield upon adding 50 mM HCO_2^-.

The effect of HCO_2^- on the prompt e_s^- yield is, we believe, best explained by the suppression of the geminate recombination reactions of electron and CH_3CNH^+ produced in reaction (3),

$$CH_3CNH^+ + e_s^- \longrightarrow CH_3CNH^{\bullet} \qquad (8)$$

occurring during the radiation spur expansion over 2-3 ns, thus increasing the homogeneous e_s^- yield, which in turn leads to an increase in the yield of $CO_2^{\bullet-}$. The suppression of reaction (8) by HCO_2^- is likely due to a combination of the inhibiting primary salt (ionic strength) effect on reaction (8) and HCO_2^- acting as a Brønsted base, scavenging CH_3CNH^+,

$$HCO_2^- + CH_3CNH^+ \longrightarrow HCO_2H + CH_3CN \qquad (9)$$

Investigation of the relative contributions from these factors is in progress.

Another significant effect of added HCO_2^- apparent in Fig. 2 is a dramatic increase in the $CO_2^{\bullet-}$ lifetime. Although the observed bi-phasic decay kinetics is not yet understood, it clearly involves more than a simple self-recombination of $CO_2^{\bullet-}$. Our working hypothesis is that the initial rapid decay is due to $CO_2^{\bullet-}$ cross-recombination with the remaining solvent radicals, and the slower decay reflects its self-recombination and, possibly, reaction with impurities including adventitious O_2.

3.4 $CO_2^{\bullet-}$ scavenging

Scavenging of $CO_2^{\bullet-}$ has been briefly investigated using a Re tricarbonyl complex (**Re**, *fac*-ReCl(bpy)(CO)$_3$) as a scavenger in order to determine the aggregate enhancement of the $CO_2^{\bullet-}$ yield by HCO_2^- and evaluate the possibility of $(CO_2)_2^{\bullet-}$ adduct formation in our systems. One-electron reduction of **Re** yields the radical species, **Re**$^{\bullet-}$, with the unpaired electron localized on the bipyridine ligand.[65] **Re**$^{\bullet-}$ is intrinsically stable on the sub-second time scale and exhibits characteristic absorption around 500 nm.[66]

The Re complex scavenges e_s^-,

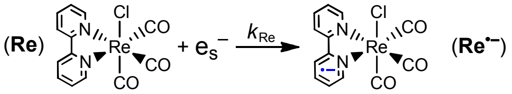

(10)

with a second-order rate constant, k_{Re} = 6.0 × 10^{10} M^{-1} s^{-1} (Fig. S6). However, with a sufficiently large [CO_2]/[**Re**] ratio, most e_s^- are intercepted by CO_2, and the reduction of **Re** occurs through the intermediacy of $CO_2^{\bullet-}$,

$$\mathbf{Re} + CO_2^{\bullet-} \xrightarrow{k_{11}} \mathbf{Re}^{\bullet-} + CO_2 \qquad (11)$$

with a rate constant, k_{11} = 5.5 × 10^9 M^{-1} s^{-1} (Fig. S7). This nearly diffusion-controlled rate is consistent with the CO_2 reduction potential being much more negative than $E°$(**Re**/**Re**$^{\bullet-}$) = –1.35 V in CH_3CN vs SCE.[65]

The kinetic data obtained under these conditions presented in Fig. 3(lower trace) show that the rapidly produced **Re**$^{\bullet-}$ decays with $t_{½} \approx 24$ µs. This kinetic trace is virtually identical to the one recorded without added CO_2 where **Re** is reduced directly by e_s^- (Fig. S8), and the decays in both cases are probably due to **Re**$^{\bullet-}$ reactions with the solvent-derived radicals and CH_3CNH^+.

With both CO_2 and HCO_2^- present, however, a much different **Re**$^{\bullet-}$ kinetics is observed (Fig. 3, upper trace). First, significantly more **Re**$^{\bullet-}$ is produced over the first 2 µs, which is expected considering the data in Fig. 2. Second, accumulation of **Re**$^{\bullet-}$ continues over the next 50 µs reaching a concentration that is 3.7 times larger than the maximum **Re**$^{\bullet-}$ concentration obtained in the absence of HCO_2^-. Because **Re**$^{\bullet-}$ reduction closely tracks the $CO_2^{\bullet-}$ production through reaction (7), this factor reflects the apparent aggregate enhancement of the $CO_2^{\bullet-}$ yield by HCO_2^-. If we accept $G(e_s^-) = 1.5 \pm 0.5$ (Table S1) and $G(R^\bullet) \approx 7$, the data in Fig. 3 would suggest that 60 ± 20% of the solvent-derived radicals are engaged in $CO_2^{\bullet-}$ generation from HCO_2^-. Experiments toward further enhancing the yield of reducing species from the solvent-derived radicals are under way.

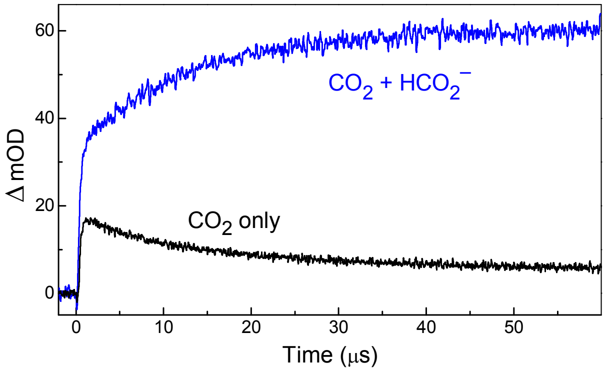

Fig. 3 Transient absorption of **Re**$^{\bullet-}$ normalized for radiation dose and recorded at 505 nm after 100 ns pulse radiolysis of deoxygenated CH_3CN containing 1 mM **Re** and: 28 mM CO_2 (lower black trace); 28 mM CO_2 and 50 mM HCO_2^- (upper blue trace). In these samples, ~95% of e_s^- are scavenged by CO_2, the e_s^- lifetime is ≈ 1 ns, and **Re**$^{\bullet-}$ is produced predominantly through reaction (11).

The $(CO_2)_2^{\bullet-}$ adduct produced via a hemicolligation reaction,

$$CO_2^{\bullet-} + CO_2 \underset{k_{-h}}{\overset{k_h}{\rightleftharpoons}} (CO_2)_2^{\bullet-} \qquad K_h = k_h/k_{-h} \qquad (12)$$

has been implicated as an intermediate of electrochemical CO_2 reduction in aprotic solvents.[24,14,25,67,27,68] Adducts of this type are well documented for aqueous halides and pseudohalides.[69] To evaluate the occurrence of reaction (12) under the experimental conditions used in this study, we have investigated the **Re**$^{\bullet-}$ absorption growth following pulse radiolysis in the presence of increasing concentrations of CO_2. As detailed in the ESI section 8, these experiments give no evidence for the occurrence of reaction (12), which can be explained either by the smallness of the hemicolligation equilibrium constant (K_h << 3.6 M^{-1}) or by the sluggishness of the hemicolligation reaction (k_h << 1×10^7 M^{-1} s^{-1}). Although we favor the latter explanation, it is clear that under the conditions of the experiments discussed throughout this paper, no appreciable amount of the $(CO_2)_2^{\bullet-}$ adduct can be generated.

4. Conclusions

Pulse radiolysis combined with TRIR spectroscopy allowed the first IR detection of $CO_2^{\bullet-}$ in CH_3CN via its antisymmetric stretch at 1650 cm^{-1}, following its formation by the scavenging of the solvated electron by dissolved CO_2. This spectral assignment was confirmed by ^{13}C isotopic labelling and DFT calculations. We have also shown that formate ion is capable of scavenging radiolytically-generated solvent-derived radicals via H-atom transfer reactions, thus providing another pathway for the formation of $CO_2^{\bullet-}$ in CH_3CN. This latter pathway is biphasic, with a prompt growth of $CO_2^{\bullet-}$ due to reaction with strongly H-atom abstracting radicals, followed by a slower growth over the next 20 µs due to the more abundant but weaker H-atom abstractor, $CH_2CN^\bullet$, which more than doubles the apparent yield of $CO_2^{\bullet-}$. In fact, preliminary experiments using a Re-based transition metal complex as an electron scavenger showed that the apparent aggregate enhancement of the $CO_2^{\bullet-}$ yield by formate is a factor of 3.7. Based on published radiation yields of e_s^- and $R^\bullet$, our data suggest that 60 ± 20% of the solvent-derived radicals are engaged in $CO_2^{\bullet-}$ generation from formate. Thus, while providing an increase in the yield of reducing species upon pulse radiolysis of CH_3CN, formate also eliminates a large fraction of the solvent radicals, resulting in a cleaner system for mechanistic investigations.

Isotopic labelling experiments also revealed that the presence of formate in solution boosts, by ~30%, the prompt yield of $CO_2^{\bullet-}$ from the scavenging of e_s^- by CO_2 (reaction (1)). This is likely due to formate suppressing the geminate recombination of e_s^- and CH_3CNH^+ (reaction (8)) by some combination of an ionic strength effect on reaction (8) and the scavenging of CH_3CNH^+ by formate (reaction (9)), thus increasing the homogeneous yield of e_s^-. Another significant effect of formate is the dramatic increase in the lifetime of $CO_2^{\bullet-}$ that it induces.

Work is under way to identify alternative radical scavengers that will further enhance the yield of reducing species from the solvent-derived radicals, and we expect TRIR detection to play an important role in these studies.

Conflicts of interest

There are no conflicts to declare.

Acknowledgements

This work, and use of the LEAF and Van de Graaff facilities of the Accelerator Center for Energy Research at BNL, was supported by the U.S. Department of Energy (DOE), Office of Science, Office of Basic Energy Sciences, Division of Chemical Sciences, Geosciences & Biosciences under contract DE-SC0012704. We thank Mr. Bobby Layne for technical support in the design and construction of TRIR detection systems at both accelerators.

Notes and references

‡ For clarity, throughout this paper the isotopic identity of the carbon atom is only explicitly stated when it is essential for distinguishing different species in an experiment.

1 At 298 K, based on 1 mol/L gaseous standard states, and $S^\circ_{298}(e^-$, 1 bar) = 5.0 kcal/(mol K), M. W. Chase, Jr., C. A. Davies, J. R. Downey, Jr., D. J. Frurip, R. A. McDonald and A. N. Syverud, *J. Phys. Chem. Ref. Data*, 1985, **14**, *Suppl.* 1.
2 R. N. Compton, P. W. Reinhardt and C. D. Cooper, *J. Chem. Phys.*, 1975, **63**, 3821-3827.
3 R. A. Holroyd, T. E. Gangwer and A. O. Allen, *Chem. Phys. Lett.*, 1975, **31**, 520-523.
4 S. Ninomiya, K. Itoh, M. Nishikawa and R. Holroyd, *J. Phys. Chem.*, 1993, **97**, 9488-9492.
5 R. A. Holroyd, K. Itoh and M. Nishikawa, *Chem. Phys. Lett.*, 1997, **266**, 227-232.
6 Calculated from reduction potentials evaluated in ref. 13.
7 P. Neta, M. Simic and E. Hayon, *J. Phys. Chem.*, 1969, **73**, 4207-4213.
8 A. Fojtik, G. Czapski and A. Henglein, *J. Phys. Chem.*, 1970, **74**, 3204-3208.
9 G. V. Buxton and R. M. Sellers, *J. Chem. Soc., Faraday Trans. 1*, 1973, **69**, 555-559.
10 R. Flyunt, M. N. Schuchmann and C. von Sonntag, *Chem. Eur. J.*, 2001, **7**, 796-799.
11 A. S. Jeevarajan, I. Carmichael and R. W. Fessenden, *J. Phys. Chem.*, 1990, **94**, 1372-1376.
12 I. Janik and G. N. R. Tripathi, *J. Chem. Phys.*, 2016, **144**, 154307.
13 D. A. Armstrong, R. E. Huie, W. H. Koppenol, S. V. Lymar, G. Merényi, P. Neta, B. Ruscic, D. M. Stanbury, S. Steenken and P. Wardman, *Pure Appl. Chem.*, 2015, **87**, 1139-1150.
14 E. Lamy, L. Nadjo and J. M. Savéant, *J. Electroanal. Chem. Interfac. Electrochem.*, 1977, **78**, 403-407.
15 P. Neta, R. E. Huie and A. B. Ross, *J. Phys. Chem. Ref. Data*, 1988, **17**, 1027-1284.
16 G. V. Buxton and Q. G. Mulazzani, in *Electron Transfer in Chemistry*, ed. V. Balzani, Wiley-VCH, Weinheim, Germany, 2001, vol. I-1, pp. 503-557.
17 G. V. Buxton, C. L. Greenstock, W. P. Helman and A. B. Ross, *J. Phys. Chem. Ref. Data*, 1988, **17**, 513-886.
18 D. C. Grills, J. A. Farrington, B. H. Layne, J. M. Preses, H. J. Bernstein and J. F. Wishart, *Rev. Sci. Instrum.*, 2015, **86**, 044102.
19 K. T. Ngo, M. McKinnon, B. Mahanti, R. Narayanan, D. C. Grills, M. Z. Ertem and J. Rochford, *J. Am. Chem. Soc.*, 2017, **139**, 2604-2618.
20 D. E. Polyansky, J. K. Hurst and S. V. Lymar, *Eur. J. Inorg. Chem.*, 2014, 619-634.
21 D. C. Grills, D. E. Polyansky and E. Fujita, *ChemSusChem*, 2017, **10**, 4359-4373.
22 D. C. Grills, A. R. Cook, E. Fujita, M. W. George, J. M. Preses and J. F. Wishart, *Appl. Spectrosc.*, 2010, **64**, 563-570.
23 D. C. Grills, J. A. Farrington, B. H. Layne, S. V. Lymar, B. A. Mello, J. M. Preses and J. F. Wishart, *J. Am. Chem. Soc.*, 2014, **136**, 5563-5566.
24 A. W. B. Aylmer-Kelly, A. Bewick, P. R. Cantrill and A. M. Tuxford, *Faraday Discuss. Chem. Soc.*, 1973, **56**, 96-107.
25 C. Amatore and J. M. Savéant, *J. Am. Chem. Soc.*, 1981, **103**, 5021-5023.
26 Y. Hori, H. Wakebe, T. Tsukamoto and O. Koga, *Electrochim. Acta*, 1994, **39**, 1833-1839.
27 A. Gennaro, A. A. Isse, M.-G. Severin, E. Vianello, I. Bhugun and J.-M. Savéant, *J. Chem. Soc., Faraday Trans.*, 1996, **92**, 3963-3968.
28 C. Costentin, M. Robert and J. M. Saveant, *Chem. Soc. Rev.*, 2013, **42**, 2423-2436.
29 D. Sun and Y. Chen, in *Electrochemical Reduction of Carbon Dioxide: Fundamentals and Technologies*, eds. J. Qiao, Y. Liu and J. Zhang, CRC Press, Boca Raton, FL, 2016, pp. 103-154.
30 D. Bradley and J. Wilkinson, *J. Chem. Soc. A*, 1967, 531-537.
31 P. B. Ayscough, H. Drawe and P. Kohler, *Radiation Res.*, 1968, **33**, 263-273.
32 A. Singh, H. D. Gesser and A. R. Scott, *Chem. Phys. Lett.*, 1968, **2**, 271-273.
33 E. Hayon, *J. Chem. Phys.*, 1970, **53**, 2353-2358.
34 J. L. Baptista and H. D. Burrows, *J. Chem. Soc., Faraday Trans. 1*, 1974, **70**, 2066-2079.
35 H. D. Burrows and E. M. Kosower, *J. Phys. Chem.*, 1974, **78**, 112-117.
36 S. W. Mao and L. Kevan, *J. Phys. Chem.*, 1976, **80**, 2330-2335.
37 I. P. Bell, M. A. J. Rodgers and H. D. Burrows, *J. Chem. Soc., Faraday Trans. 1*, 1977, **73**, 315-326.
38 T. H. Tran-Thi, A. M. Koulkes-Pujo, L. Gilles, M. Genies and J. Sutton, *Radiat. Phys. Chem.*, 1980, **15**, 209-214.
39 S. Mosseri, P. Neta and D. Meisel, *Radiat. Phys. Chem.*, 1990, **36**, 683-687.
40 S. Nagahara, T. Kozawa, Y. Yamamoto and S. Tagawa, *J. Photopolym. Sci. Tech.*, 1998, **11**, 577-580.
41 Y.-R. Luo, *Comprehensive Handbook of Chemical Bond Energies*, CRC Press, Boca Raton, 2007.
42 R. H. Schuler, P. Neta and G. R. Holdren, *J. Phys. Chem.*, 1971, **75**, 449-454.
43 I. Draganic, Z. Draganic, L. Petkovic and A. Nikolic, *J. Am. Chem. Soc.*, 1973, **95**, 7193-7199.

44 B. Wang, H. Hou and Y. Gu, *J. Phys. Chem. A*, 2001, **105**, 156-164.
45 I. A. Shkrob and M. C. Sauer, *J. Phys. Chem. A*, 2002, **106**, 9120-9131.
46 C. G. Xia, J. Peon and B. Kohler, *J. Chem. Phys.*, 2002, **117**, 8855-8866.
47 S. C. Doan and B. J. Schwartz, *J. Phys. Chem. Lett.*, 2013, **4**, 1471-1476.
48 S. C. Doan and B. J. Schwartz, *J. Phys. Chem. B*, 2013, **117**, 4216-4221.
49 T. Imamura, T. Sumiyoshi, K. Takahashi and Y. Sasaki, *J. Phys. Chem.*, 1993, **97**, 7786-7791.
50 V. Samant, A. K. Singh, T. Mukherjee and D. K. Palit, *Res. Chem. Intermed.*, 2006, **32**, 767-776.
51 E. A. Cherniak, E. Collinson, F. S. Dainton and G. M. Meaburn, *Proc. Chem. Soc.*, 1958, 54.
52 G. H. Miller and J. J. Martin, *Ann. N.Y. Acad. Sci.*, 1963, **105**, 629-646.
53 M. Wrighton and D. L. Morse, *J. Am. Chem. Soc.*, 1974, **96**, 998-1003.
54 A. Gennaro, A. A. Isse and E. Vianello, *J. Electroanal. Chem.*, 1990, **289**, 203-215.
55 M. Lin, Y. Katsumura, Y. Muroya, H. He, T. Miyazaki and D. Hiroishi, *Radiat. Phys. Chem.*, 2008, **77**, 1208-1212.
56 M. E. Jacox and W. E. Thompson, *J. Chem. Phys.*, 1989, **91**, 1410-1416.
57 W. E. Thompson and M. E. Jacox, *J. Chem. Phys.*, 1999, **111**, 4487-4496.
58 M. F. Zhou and L. Andrews, *J. Chem. Phys.*, 1999, **110**, 2414-2422.
59 K. O. Hartman and I. C. Hisatsune, *J. Chem. Phys.*, 1966, **44**, 1913-1918.
60 I. C. Hisatsune, T. Adl, E. C. Beahm and R. J. Kempf, *J. Phys. Chem.*, 1970, **74**, 3225-3231.
61 K. Bobrowski and P. K. Das, *J. Phys. Chem.*, 1985, **89**, 5733-5738.
62 K. Bobrowski, G. Dzierzkowska, J. Grodkowski, Z. Stuglik, Z. P. Zagorski and W. L. McLaughlin, *J. Phys. Chem.*, 1985, **89**, 4358-4366.
63 S. Nad and H. Pal, *J. Chem. Phys.*, 2002, **116**, 1658-1670.
64 J. R. De la Fuente, G. Kciuk, E. Sobarzo-Sanchez and K. Bobrowski, *J. Phys. Chem. A*, 2008, **112**, 10168-10177.
65 B. P. Sullivan, C. M. Bolinger, D. Conrad, W. J. Vining and T. J. Meyer, *J. Chem. Soc., Chem. Commun.*, 1985, 1414-1415.
66 K. Kalyanasundaram, *J. Chem. Soc., Faraday Trans. 2*, 1986, **82**, 2401-2415.
67 Y. B. Vassiliev, V. S. Bagotzky, O. A. Khazova and N. A. Mayorova, *J. Electroanal. Chem. Interfac. Electrochem.*, 1985, **189**, 295-309.
68 D. A. Tryk, T. Yamamoto, M. Kokubun, K. Hirota, K. Hashimoto, M. Okawa and A. Fujishima, *Appl. Organomet. Chem.*, 2001, **15**, 113-120.
69 See, for example, Table 4 in ref. 13.